# Strain-Tunable Magnetic Moment in Ni-Doped Graphene Monolayer.

**Published in:**
Journal of Physical Chemistry C

**Document Version:**
Peer reviewed version

**Queen's University Belfast - Research Portal:**
[Link to publication record in Queen's University Belfast Research Portal](#)

# Strain-Tunable Spin Moment in Ni-Doped Graphene

Elton J. G. Santos,[†,‡] A. Ayuela,[†,‡] and D. Sánchez-Portal[∗,†,‡]

*Centro de Física de Materiales (CFM-MPC), Centro Mixto CSIC-UPV/EHU, Paseo Manuel de Lardizabal 5, 20018 San Sebastián, Spain, and Donostia International Physics Center (DIPC), Paseo Manuel de Lardizabal 4, 20018 San Sebastián, Spain*

E-mail: sqbsapod@ehu.es

KEYWORDS: Graphene, Impurities, Doping, Nickel, Uniaxial Strain, DFT

---

[∗]To whom correspondence should be addressed

[†]Centro de Física de Materiales (CFM-MPC), Centro Mixto CSIC-UPV/EHU, Paseo Manuel de Lardizabal 5, 20018 San Sebastián, Spain

[‡]Donostia International Physics Center (DIPC), Paseo Manuel de Lardizabal 4, 20018 San Sebastián, Spain

**Abstract**

Graphene, due to its exceptional properties, is a promising material for nanotechnology applications. In this context, the ability to tune the properties of graphene-based materials and devices with the incorporation of defects and impurities can be of extraordinary importance. Here we investigate the effect of uniaxial tensile strain on the electronic and magnetic properties of graphene doped with substitutional Ni impurities ($Ni_{sub}$). We have found that, although $Ni_{sub}$ defects are non-magnetic in the relaxed layer, uniaxial strain induces a spin moment in the system. The spin moment increases with the applied strain up to values of 0.3-0.4$\mu_B$ per $Ni_{sub}$, until a critical strain of $\sim$6.5% is reached. At this point, a sharp transition to a high-spin state ($\sim$1.9 $\mu_B$) is observed. This magnetoelastic effect could be utilized to design strain-tunable spin devices based on Ni-doped graphene.

# Introduction

The special electronic and magnetic properties of graphene have led to the proposal of new types of electronic and spintronic devices based on this material.[1–7] For this purpose, it is instrumental to study the impact of defects and impurities on such properties. Defects can deteriorate the performance of graphene-based devices. However, defects and impurities can also be used to tune the electronic, magnetic and mechanical properties of those devices and, therefore, be intentionally incorporated in the structure. This has driven an increasing attention to defects in graphene.[8] Both intrinsic defects[9,10] and extrinsic defects, like substitutional atoms,[11–14] are presently under intense research. In this context, substitutional metal impurities seem particularly attractive. Recent experiments indicate that metal atoms can be easily incoporated in the graphenic layer as substitutional dopants at predefined positions. Carbon vacancies can be created in graphene and carbon nanotubes by focusing an electron beam using scanning transmission electron microscope. Metal atoms migrating on the graphenic surfaces are then observed to be trapped in such defects with bonding energies of several eVs.[15,16] This opens a route to fabricate stable arrays of substitutional impurities that may allow for the exploration of the interesting magnetic and electronic properties

predicted for such systems.[11,12]

Ni substitutional impurities (Ni$_{sub}$) have been experimentally detected in single-walled carbon nanotubes (SWCNTs)[17] and large fullerenes and graphitic particles.[18] Theoretical studies on the magnetic properties of these defects revealed surprising results. While Ni$_{sub}$ impurities are non-magnetic in flat graphene,[13,14] they can develop a substantial spin-moment (up to ∼0.8 $\mu_B$) in metallic SWCNTs.[11] This peculiar behavior stems from the curvature dependence of the electronic structure of Ni$_{sub}$ defects. Therefore, in Ref.[11] it was proposed that curvature could be used to switch on the magnetism of Ni$_{sub}$ impurities in metallic graphenic nanostructures. Unfortunately, the local curvature at the location of the Ni$_{sub}$ defect cannot be easily determined and controlled in experiments.

For this reason, in the present paper we explore a different way to modify the local geometry and, consequently, the electronic and magnetic properties of Ni$_{sub}$ impurities. Here, we study the effect of uniaxial tensile strain on graphene layers doped with Ni$_{sub}$ defects. As we will see in detail below, we have found that uniaxial strain can be used to induce a transition of the Ni$_{sub}$ defect to a magnetic state and, thus, to tune the magnetic properties of Ni-doped graphene. At moderate strains, Ni$_{sub}$ defects develop a spin moment that slowly increases with strain up to values of 0.3-0.4$\mu_B$. The change is more dramatic when a critical strain of ∼6.5% is reached: An abrupt increase of the spin moment to ∼1.9 $\mu_B$ is observed. This magnetoelastic effect could be utilized to design strain-tunable spin devices based on Ni-doped graphene.

Substitutional transition metal impurities in graphene and, in general, small clusters of transition metals interacting with graphenic layers are likely sites for the adsorption of molecules.[19,20] For example, the possible catalytic activity of Au atoms embedded in graphene for CO oxidation has been theoretically studied.[21] Experiments have also found an enhanced catalytic activity of this oxidation reaction for sub-nanometer Pt clusters deposited on graphene.[20] There are also recent calculations of oxygen interacting with Cr and Mn substitutionals in graphene.[22] The spin moment of these impurities change after the adsorption of the molecule and this possibility should be taken into account when comparing the present results with measurements under ambient con-

ditions. An additional complication is that the reactivity of the impurities is likely to depend on the applied strain.[23,24] Therefore, we restrict our study to the evolution of the spin moment for substitutionally Ni-doped graphene under vacuum conditions as a function of a well-defined external parameter, the applied uniaxial strain.

## Methods

To theoretically investigate the problem we have carried out first-principles density-functional calculations of $Ni_{sub}$ defects in graphene under uniaxial strains in an experimentally accessible range.[25,26] The calculations have been performed using the SIESTA code[27] and the PBE-GGA functional.[28] We have used a rectangular supercell containing 111 C atoms and a single $Ni_{sub}$ impurity. The carbon layers are always separated by a distance of at least 17 Å, so that the interaction between adjacent layers is negligible. Stresses of different magnitudes are applied along the $(n, n)$ and $(n, 0)$ directions, and both atomic coordinates and lattice vectors are allowed to relax.[29] A double-$\zeta$ polarized (DZP)[27] basis set has been always used for the calculation of the magnetic and electronic properties. However, we have checked that using a double-$\zeta$ (DZ) basis set yields almost identical relaxed structures and spin moments as the DZP basis and, therefore, we have used the smaller DZ basis for most structural relaxations. Other computational parameters are similar to those used in our previous work on $Ni_{sub}$ impurities in SWCNTs[11] and graphene.[13] We have also performed GGA+U calculations at different values of the strain using the formulation of Dudarev *et al.*[30] and several values of the U parameter varied in the range 1-4 eV. GGA+U results did not show significant deviations from PBE-GGA calculations and, thus, here we only present the latter.

## Results and Discussion

[figure][1][]1 shows the spin moment of a $Ni_{sub}$ defect as a function of the strain applied along the $(n, n)$ (a) and $(n, 0)$ (b) directions. Open and filled squares show results obtained using geometries relaxed with and without spin polarization, respectively. These relaxations utilized a DZ
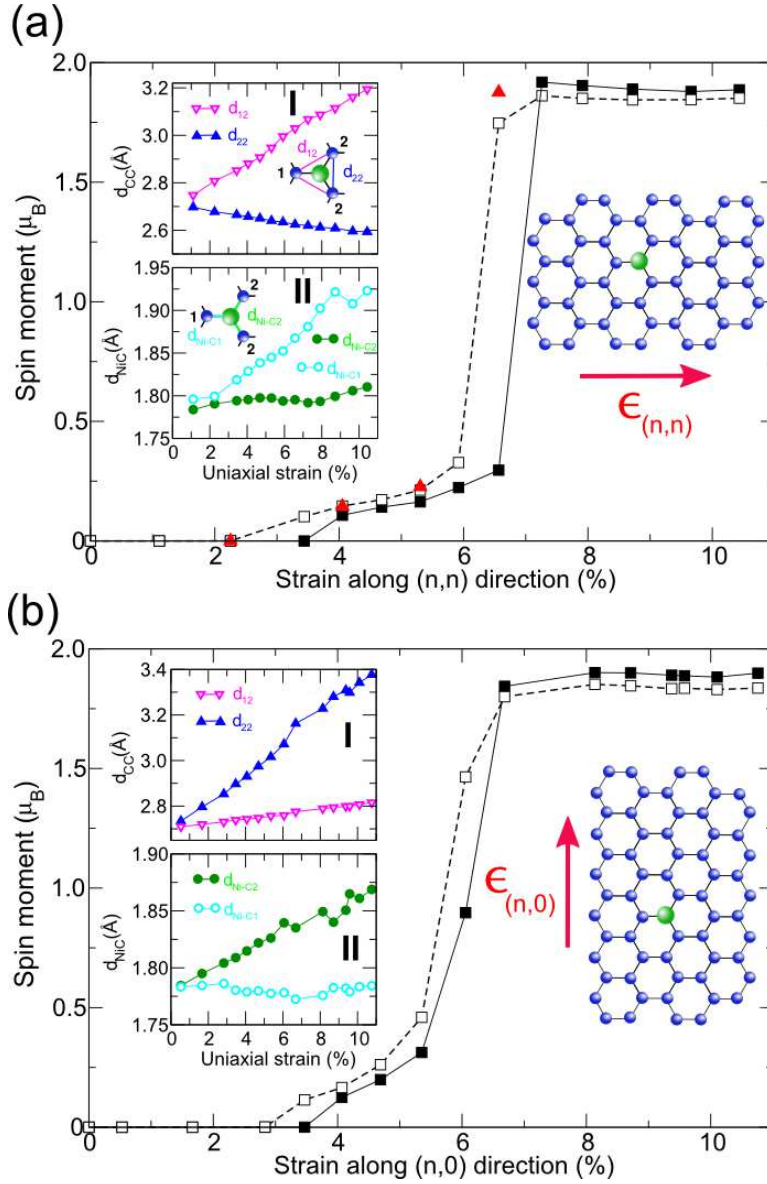
Figure 1: (Color online) Spin moment of a $Ni_{sub}$ impurity in graphene as a function of the applied strain ($\varepsilon$) along the $(n,n)$ (a) and $(n,0)$ (b) directions. A schematic illustration of the structure is included. In panels (a) and (b), filled squares indicate results obtained using geometries from a non-spin polarized calculation using a DZ basis. The electronic structure and spin moment are calculated using a more complete DZP basis using such geometry. Open squares indicate a similar calculation, but the geometries come from a spin-polarized calculation in this case. The triangles represent a calculation where both the relaxed geometry and the spin moment have been obtained using a DZP basis set. Insets I and II in panels (a) and (b) show the distances between carbon atoms C1 and C2 ($d_{12,22}$) and Ni-C bond lenghts ($d_{Ni-C1, Ni-C2}$) as a function of the applied uniaxial strain calculated using a DZ basis set and spin polarization.

5

basis set, although the spin moments in [figure][1][]1 were always computed using the more complete DZP basis. The triangles display calculations where the geometry was obtained using a DZP basis set and spin polarization. The relaxed structures and the behavior of the spin moment as a function of the uniaxial strain are very similar in all the cases. At zero strain the $Ni_{sub}$ defect is non-magnetic as was previously reported and analyzed in earlier studies.[11,13] The structure around the defect deforms as the uniaxial tension is applied (see the insets in [figure][1][]1). As a consequence, the electronic structure of the defect is modified and a spin moment develops. We see that at ~3.5% strain the system becomes magnetic with a spin moment that increases slowly with the uniaxial strain up to values of ~0.30-0.40 $\mu_B$ for a strain of ~6.0%. At ~6.5% strain, the spin moment increases sharply to ~1.9 $\mu_B$ and remains almost constant for larger strains. This means that a moderate variation of the strain applied on the layer can induce a large change of the spin moment associated with the $Ni_{sub}$ defects. This is particularly attractive in connection with recent experimental reports that indicate that metal atoms can be easily incorporated in graphene as substitutional dopants, even at predefined position.[15,16] Therefore, the present results can, in principle, be used to design a new family of magnetoelastic devices based on graphene. Furthermore, if uniaxial strain is varied in a larger scale similar to the one presented in [figure][1][]1, the magnetism of Ni-doped graphene can be switched on and off at will. Since according to recent experiments[25,26] uniaxial strain can be applied on graphene in a controlled way, our results are suitable for experimental verification.

The transition to a high-spin solution in [figure][1][]1 is similar for both strain orientations, although somewhat more abrupt for the $(n,n)$ direction (panel (a)) where no intermediate steps are observed. This small difference already points to the role played on the development of the spin moment by the local defect geometry and its orientation relative to the applied strain. Insets I and II in [figure][1][]1(a) and (b) present this geometrical information. When the strain is applied, the largest deformation corresponds to the triangle formed by the three C neighbors of the $Ni_{sub}$ impurity. As expected, the variation of the three C-C distances ($d_{C-C}$) is different depending on their orientation relative to the strain direction. The length of those C-C bonds pointing along the

6

strain direction increases, whereas those pointing along the perpendicular direction are reduced by a much smaller amount. This corresponds to the expected elastic behavior for graphene, and can be understood as a tendency to keep approximately a constant area per atom. As we will see below, this distortion strongly affects the position of the defect levels associated with the Ni$_{sub}$ impurity. The Ni-C bonds (d$_{Ni-C}$) also increase on average. However, for the studied range of strains up to $\sim$10.5%, the maximum increase of d$_{Ni-C}$ is $\sim$8% whereas it is as large as $\sim$25% for d$_{C-C}$. This difference is partially explained by the elevated position of the Ni atom over the graphene layer, that provides an additional degree of freedom to respond to the layer elongation. The Ni atom is larger than the C atom that was removed to create the vacancy, thus it moves out of the carbon plane. At zero strain its height over the carbon layer is $\sim$0.9 Å. This height decreases as a function of the applied strain (by as a much as 17% for the maximum strain applied here). In spite of its elevated position, the Ni atom is strongly bound to the C vacancy with a large binding energy of about 7 eV,[13] which clearly ensures its chemical stability.

In order to understand the origin of the tunable spin-moment of Ni$_{sub}$ defects in graphene, the densities of states (DOS) for spin-unpolarized calculations under 0.0%, 2.2%, 5.3% and 7.2% strain along the $(n,n)$ direction are shown in [figure][2][]2 (a). The qualitative behavior is similar if the strain is applied along other directions. At zero strain we find two sharp peaks around the Fermi energy (E$_F$). They correspond to a singly- and a doubly-degenerate defect level, respectively. The character of these levels was analyzed in detail in Ref.[13] They mainly come from the hybridization of the Ni $3d$ orbitals with the neighboring C atoms. Due to the symmetric position of the metal atom over the vacancy, the system has a $C_{3v}$ symmetry at zero strain and the electronic levels can be classified according to the $A$ or $E$ irreducible representations of this point group. The position of these defect states as a function of the applied strain determines the observed behavior of the spin moment.

One of the levels, with $A$ character, is occupied and appears around $\sim$0.5 eV below E$_F$ at zero strain. This state comes from a fully symmetric linear combination of the $2p_z$ orbitals (z-axis normal to the layer) of the nearest C neighbors interacting with the $3d_{z^2}$ orbital of Ni. The
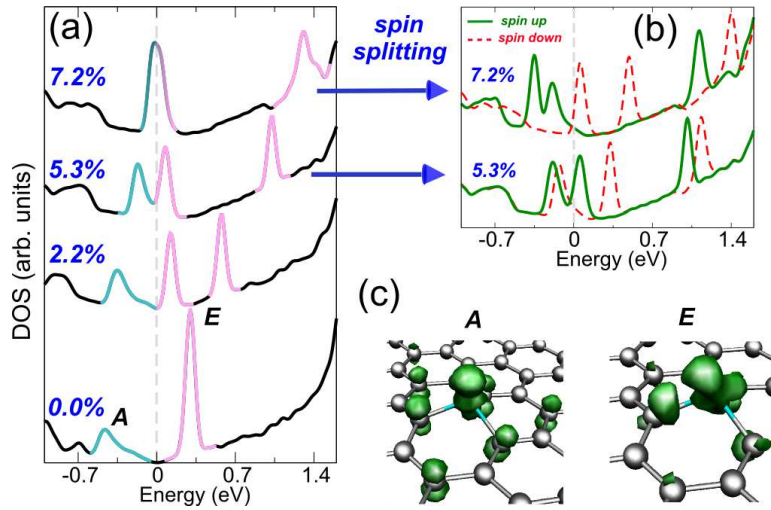
Figure 2: (Color online) (a) Spin-unpolarized density of states (DOS) of a $Ni_{sub}$ impurity in graphene under uniaxial strains of $0.0\%$, $2.2\%$, $5.3\%$ and $7.2\%$ along the $(n,n)$ direction. Symbols $A$ and $E$ indicate the symmetry of the defect levels coming from the hybridization of Ni and the neighboring C atoms at zero strain. The level $A$ corresponds to a Ni $3d_{z^2}-$C $2p_z$ hybridization and the levels $E$ have a Ni $3d_{xz}, 3d_{yz}-$C $2sp$ character. (b) Spin-polarized DOS showing the spin splitting and the occupations of the different levels at strains of $5.3\%$ and $7.2\%$. Solid (green) and dashed (red) lines stand for majority and minority spins, respectively. Different curves in panels (a) and (b) have been shifted for clarity. The Fermi energy is marked by the dashed vertical line and is set to zero. (c) Density associated with the $A$ and the lowest $E$ levels at a strain of $5.3\%$ with an isovalue of $\pm 0.002$ e$^-$/Bohr$^3$ (spin-unpolarized calculation).

other twofold-degenerate level, with $E$ character, comes from the hybridization of the in-plane $sp$ lobes of the carbon neighbors with the Ni $3d_{xz}$ and $3d_{yz}$ orbitals and appears at 0.4 eV above $E_F$ at zero strain. As a consequence of this electronic structure, with the Ni $3d$ states far from $E_F$ and no flat bands crossing $E_F$, the magnetic moment of the $Ni_{sub}$ impurity in graphene is zero. Interestingly, these levels appearing close to $E_F$ in [figure][2][]2(a) are reminiscent of those found for the unreconstructed carbon vacancy in graphene.[9,13]

The energy position of these three levels shifts as a function of the applied strain. This can be clearly seen in [figure][2][]2 (a). When a finite strain is applied, the degeneracy between Ni $3d_{xz}-$C $2sp$ and Ni $3d_{yz}-$C $2sp$ states ($E$ levels) is removed and one of them gradually shifts towards $E_F$. The fully-occupied Ni $3d_{z^2}-$C $2p_z$ state (with $A$ symmetry) also moves towards $E_F$ as a function of the strain, although at a somewhat smaller pace. For small strains (above $\sim$3.5%) the lowest $E$ level becomes partially populated. At somewhat larger strains ($\sim$5%), the $A$ level is also sufficiently close to $E_F$ so it starts to lose a small part of its charge. This population is transferred to the lowest $E$ level, so the occupations of these two levels change without an appreciable modification of the total charge localized around the Ni impurity. Finally, around 6.5% strain both, the $A$ state and the lowest $E$ level, become half-occupied. This exchange of population between the $A$ and lowest $E$ levels is the mechanism behind the sharp transition of the spin moment observed in the calculations. Eventually both levels become half-occupied, so they polarize and the system develops a spin moment of 2 $\mu_B$.

This can be seen more clearly in [figure][2][]2 (b), which presents the spin-polarized DOS for two strains around the transition point. Closely below the transition, at 5.3% strain, the lowest $E$ level is partially populated, developing a small spin polarization. Simultaneously, the fully-occupied $A$ level starts to lose part of its population, although presents an almost negligible spin polarization. The corresponding exchange splittings are $\sim$0.29 eV and $\sim$0.13 eV for the $E$ levels and only $\sim$0.05 eV for the $A$ state. The larger splitting and corresponding polarization of the $E$ levels is related to their larger localization. The spatial distribution of the density associated with the $A$ level and the lowest $E$ level can be seen in [figure][2][]2 (c). The different localization and

symmetry of the two states, as well as the antibonding nature of the interaction between Ni and the neighboring C atoms, is manifest in these plots. Above the transition, for example at 7.2% strain in [figure][2][]2 (c), we can see that both levels, $A$ and the lowest $E$, are fully polarized. Accordingly, the spin splittings increase considerably: $\sim$0.86 eV and $\sim$0.34eV for the $E$ states and $\sim$0.25 eV for the A level. The stability of the spin-polarized solutions with respect to the non-magnetic solutions is also enhanced from 14 meV per Ni atom at 5.3% strain to 184 meV at 7.2% strain.
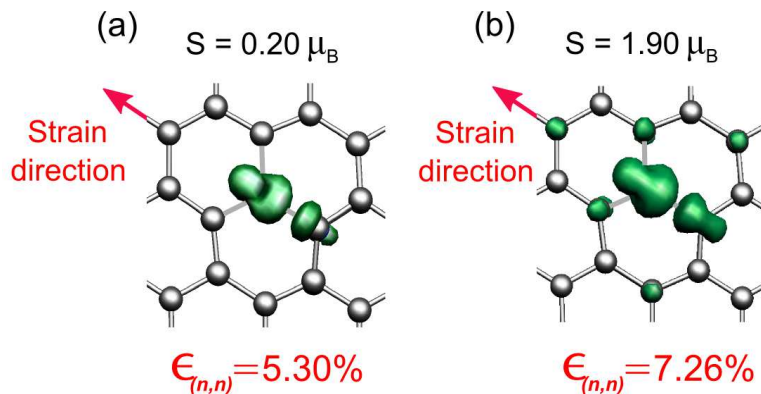


Figure 3: (Color online) (a)-(b) Spin densities for Ni$_{sub}$ defects in graphene at strains of 5.30% and 7.2% along the $(n,n)$ direction. The strain direction is marked by the red arrows in both panels. The isovalue cutoff in (a) and (b) panels is $\pm$0.035 and $\pm$0.060 e$^-$/Bohr$^3$, respectively.

The changes of the spin-polarization when moving across the transition at $\sim$6.5% strain are depicted in [figure][3][]3. The spin polarization in the neighboring carbon atoms depends on the strain intensity. At 5.30% strain, the spin density is mainly localized at the Ni impurity and at the C atom directly bonded to it along the strain direction. The magnetization density reflects the anti-bonding character of this $E$ defect state, as seen in the node along the bond. The $2sp$-like shape of the spin density around the C atom is also clear. This should be contrasted with the spin distribution at 7.2% strain. At this larger value of the strain, the spin density presents an additional $2p_z$ component on the neighboring carbon atoms. This substantial modification of the spin density confirms the contribution from the Ni $3d_{z^2}$$-$C $2p_z$ defect level for strains above $\sim$6.5%, as already expected from the analysis presented in [figure][2][]2.

According to our interpretation, the moderate polarization of the Ni$_{sub}$ defect in flat graphene as a function of the applied uniaxial strain below $\sim$6.5% strain is clearly reminiscent of the curvature-

induced spin-polarization found in $Ni_{sub}$-doped SWCNTs.[11] In that case, it was shown that the curvature of the carbon wall in SWCNTs was able to break the degeneracy of the two unoccupied $E$-symmetry defect levels of the $Ni_{sub}$ impurities. For sufficiently large curvatures, in the case of metallic tubes, one of these levels would become partially populated and induce the spin polarization of the $Ni_{sub}$-SWCNT system. However, there are a number of differences between the present case and that of SWCNTs. One of them is that, due to the reduced density of states near $E_F$ in graphene, the spin-polarization is more localized in the case of flat graphene under uniaxial strain. Another important difference is that the spin moment of $Ni_{sub}$ in graphene can, at least in principle, be easily tuned since the degree of strain applied to the layer can be controlled.[25,26] Finally, in the case of graphene under tensile strain, for strains above a $\sim$6.5% the $Ni_{sub}$ defects present a high-spin state that was not found in the case of the curvature-induced magnetism.

## Conclusions

In summary, our first-principles calculations show that the electronic and magnetic structure of substitutional Ni defects in graphene can be tuned with the use of uniaxial strain. While $Ni_{sub}$ defects are predicted to be non-magnetic for the unstrained layer, we observe that by stretching the layer by a few percents it is possible to turn their magnetism on. The spin moment increases slowly with the applied strain until a critical value ($\sim$6.5%) is reached. At this value, the spin moment exhibits a sharp transition to a higher value of $\sim$1.9 $\mu_B$ and remains almost constant as the strain is futher increased. This result is consistent with a very recent report by Huang *et al.*[31] using a different computational methodology. According to our calculations, this behavior of the spin moment is weakly dependent on the orientation of the applied strain. A detailed analysis indicates that this strain-tunable spin moment results from changes in the position of three defect levels around the Fermi energy which are antibonding combinations of the Ni $3d$ states and the $2p_z$ and $2sp$ orbitals of the neighboring C atoms. This tunable magnetism observed in $Ni_{sub}$ defects may be interesting for spintronic devices based on graphene.

# Acknowledgements

## Notes and References

(1) Novoselov, K. S.; Geim, A. K.; Morozov, S. V.; Jiang, D.; Zhang, Y.; Dubonos, S. V.; Grigorieva, I. V.; Firsov, A. A. *Science* **2004**, *306*, 666–669.

(2) Novoselov, K. S.; Geim, A. K.; Morozov, S. V.; Jiang, D.; Katsnelson, M. I.; Grigorieva, I. V.; Dubonos, S. V.; Firsov, A. A. *Nature* **2005**, *438*, 197–199.

(3) Son, Y.-W.; Cohen, M. L.; Louie, S. G. *Nature* **2006**, *444*, 347–349.

(4) Geim, A. K.; Novoselov, K. S. *Nature Materials* **2007**, *6*, 183–191.

(5) Park, C.-H.; Yang, L.; Son, Y.-W.; Cohen, M. L.; Louie, S. G. *Nature Physics* **2008**, *4*, 213–217.

(6) Castro Neto, A. H.; Guinea, F.; Peres, N. M. R.; Novoselov, K. S.; Geim, A. K. *Rev. Mod. Phys.* **2009**, *81*, 109–162.

(7) Geim, A. K. *Science* **2009**, *324*, 1530–1534.

(8) Banhart, F.; Kotakoski, J.; Krasheninnikov, A. *ACS Nano* **2011**, *5*, 26–41.

(9) Amara, H.; Latil, S.; Meunier, V.; Lambin, P.; Charlier, J.-C. *Phys. Rev. B* **2007**, *76*, 115423.

(10) Lehtinen, P. O.; Foster, A. S.; Ayuela, A.; Krasheninnikov, A. V.; Nordlund, K.; Nieminen, R. *Phys. Rev. Lett.* **2003**, *91*, 017202.

(11) Santos, E. J. G.; Ayuela, A.; Fagan, S. B.; Filho, J. M.; Azevedo, D. L.; Filho, A. G. S.; Sánchez-Portal, D. *Phys. Rev. B* **2008**, *78*, 195420.

(12) Santos, E. J. G.; Sánchez-Portal, D.; Ayuela, A. *Phys. Rev. B* **2010**, *81*, 125433.

(13) Santos, E. J. G.; Ayuela, A.; Sánchez-Portal, D. *New Journal of Physics* **2010**, *12*, 053012.

(14) Krasheninnikov, A. V.; Lehtinen, P. O.; Foster, A. S.; Pyykkö, P.; Nieminen, R. M. *Phys. Rev. Lett.* **2009**, *102*, 126807.

(15) Rodríguez-Manzo, J. A.; Cretu, O.; Banhart, F. *ACS Nano* **2010**, *4*, 3422–3428.

(16) Cretu, O.; Krasheninnikov, A. V.; Rodríguez, J. A.; Sun, L.; Nieminen, R.; Banhart, F. *Phys. Rev. Lett.* **2010**, *105*, 196102.

(17) Ushiro, M.; Uno, K.; Fujikawa, T.; Sato, Y.; Tohji, K.; Watari, F.; Chun, W. J.; Koike, Y.; Asakura, K. *Phys. Rev. B* **2006**, *73*, 144103.

(18) Banhart, F.; Charlier, J. C.; Ajayan, P. M. *Phys. Rev. Lett.* **2000**, *84*, 686–689.

(19) García-Lastra, J. M.; Mowbray, D. J.; Thygesen, K. S.; Rubio, A.; Jacobsen, K. W. *Phys. Rev. B* **2010**, *81*, 245429.

(20) Yoo, E.; Okata, T.; Akita, T.; Kohyama, M.; Nakamura, J.; Honma, I. *Nano Letters* **2009**, *9*, 2255–2259.

(21) Lu, Y.-H.; Zhou, M.; Zhang, C.; Feng, Y.-P. *The Journal of Physical Chemistry C* **2009**, *113*, 20156–20160.

(22) Dai, J.; Yuan, J. *Phys. Rev. B* **2010**, *81*, 165414.

(23) Zhou, M.; Zhang, A.; Dai, Z.; Feng, Y. P.; Zhang, C. *J. Phys. Chem. C* **2010**, *114*, 16541–16546.

(24) Zhou, M.; Lu, Y.; Zhang, C.; Feng, Y. P. *Appl. Phys. Lett.* **2010**, *97*, 103109.

(25) Mohiuddin, T. M. G.; Lombardo, A.; Nair, R. R.; Bonetti, A.; Savini, G.; Jalil, R.; Bonini, N.; Basko, D. M.; Galiotis, C.; Marzari, N.; Novoselov, K. S.; Geim, A. K.; Ferrari, A. C. *Phys. Rev. B* **2009**, *79*, 205433.

(26) Kim, K. S.; Zhao, Y.; Houk, J.; Lee, S. Y.; Kim, J. M.; Kim, K. S.; Ahn, J. H.; Kim, P.; Choi, J. Y.; Hong, B. H. *Nature* **2009**, *457*, 706–710.

(27) Soler, J. M.; Artacho, E.; Gale, J. D.; García, A.; Junquera, J.; Ordejón, P.; Sánchez-Portal, D. *J. Phys.: Condensed Matter* **2002**, *14*, 2745–2779.

(28) Perdew, J. P.; Burke, K.; Ernzerhof, M. *Phys. Rev. Lett.* **1996**, *77*, 3865–3868.

(29) From our calculations we can extract the Young modulus (E) and the Poisson ratio ($\nu$) of the system. For pristine graphene we obtain E=57 eV/atom and $\nu$=0.15 in good agreement with other calculations and the experimental data.[32] The Ni$_{sub}$ impurity in our supercell has a small impact on these parameters, we obtain E$\sim$55 eV/atom and $\nu \sim$0.17 for the Ni-doped layer.

(30) Dudarev, S. L.; Botton, G. A.; Savrasov, S. Y.; Humpreys, C. J.; Sutton, A. P. *Phys. Rev. B* **1998**, *57*, 1505–1509.

(31) Huang, B.; Yu, J. J.; Wei, S. H. *Phys. Rev. B* **2011**, *84*, 075415.

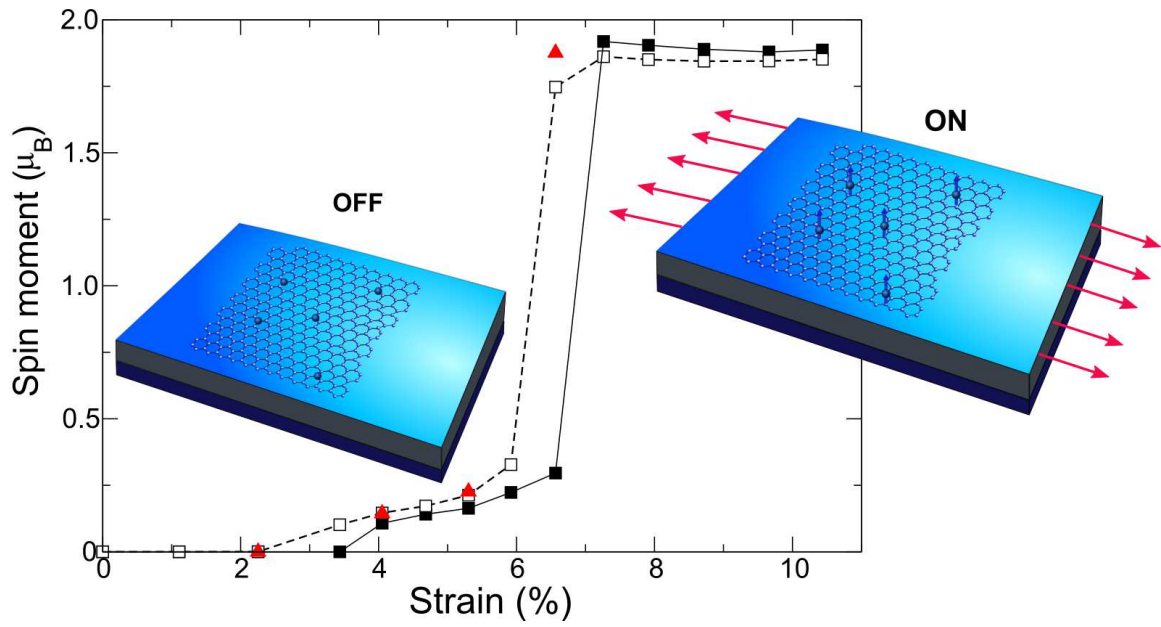(32) Sánchez-Portal, D.; Artacho, E.; Soler, J. M.; Rubio, A.; Ordejón, P. *Phys. Rev. B* **1999**, *59*, 12678–12688.

Figure 4: TOC